(NASA-TM-111201)   ELEVATED
TEMPERATURE AXIAL AND TORSIONAL
FATIGUE BEHAVIOR OF HAYNES 188
(NASA. Lewis Research Center)   9 p

N96-17778

Unclas

G3/26   0098247

REPRINT
IN-26-TM
7175
P. 9

Elevated Temperature Axial and Torsional Fatigue Behavior of Haynes 188

Peter J. Bonacuse

Research Engineer,
Vehicle Propulsion Directorate;
U.S. Army Research Laboratory,
NASA Lewis Research Center,
Cleveland, OH 44135

Sreeramesh Kalluri

Senior Research Engineer,
NYMA, Inc.,
NASA Lewis Research Center,
Cleveland, OH 44135

The results are reported for high-temperature axial and torsional low-cycle fatigue experiments performed at 760°C in air on thin-walled tubular specimens of Haynes 188, a wrought cobalt-base superalloy. Data are also presented for mean coefficient of thermal expansion, elastic modulus, and shear modulus at various temperatures from room to 1000°C, and monotonic and cyclic stress-strain curves in tension and in shear at 760°C. This data set is used to evaluate several multiaxial fatigue life models (most were originally developed for room temperature multiaxial life prediction) including von Mises equivalent strain range (ASME Boiler and Pressure Vessel Code), Manson-Halford, Modified Multiaxiality Factor (proposed in this paper), Modified Smith-Watson-Topper, and Fatemi-Socie-Kurath. At von Mises equivalent strain ranges (the torsional strain range divided by $\sqrt{3}$, taking the Poisson's ratio to be 0.5), torsionally strained specimens lasted, on average, factors of 2 to 3 times longer than axially strained specimens. The Modified Multiaxiality Factor approach shows promise as a useful method of estimating torsional fatigue life from axial fatigue data at high temperatures. Several difficulties arose with the specimen geometry and extensometry used in these experiments. Cracking at extensometer probe indentations was a problem at smaller strain ranges. Also, as the largest axial and torsional strain range fatigue tests neared completion, a small amount of specimen buckling was observed.

Introduction

In high-temperature environments it is rare to find an actual working component that is subjected to a purely uniaxial stress or strain field. Typically, when a structure is exposed to an external heat source, the heated portion expands while portions of the structure that are farther from the heat source, and cooler, constrain this expansion. In many cases a thermal gradient in a structure induces biaxial stress fields. The stresses resulting from "self-constraint" can also be amplified by external constraints on the structure. These thermally induced stresses are often accompanied by mechanical loads (e.g., centrifugal and pressure loads on a gas turbine blade) that have a different magnitude and direction than the thermal stresses. An added complexity is introduced when the thermal loads and the mechanical loads are not imposed simultaneously. This can cause the magnitudes and the directions of the maximum principal stresses and strains to change continuously during each loading cycle. Synergistic and previously undiscovered damage mechanisms may arise under these complicated loading conditions.

Haynes 188 was chosen as a model material for this study because it is often used in aeronautical and space-based, high thermal-shock applications: in LOX (liquid oxygen) posts in the space shuttle main engine, in combustors for the T800 turboshaft engine, and in other structures that are subjected to large thermal transients in oxidizing environments.

In this program, monotonic and cyclic axial and torsional tests were conducted on Haynes 188 at 760°C. Several multiaxial fatigue life prediction models were examined for their applicability to Haynes 188 at this temperature. These models include the von Mises equivalent strain range approach (ASME Boiler and Pressure Vessel Code, Case 1592-7, 1975); a method originally developed by Manson and Halford (1977); the Modified Multiaxiality Factor approach described in this report; the Modified Smith-Watson-Topper parameter (Socie, 1987 and Smith et al., 1970); and a multiaxial fatigue life model developed by Fatemi and Socie (1988) and Fatemi and Kurath (1988). The Fatemi-Socie-Kurath model is actually a correlation for this data set in that it requires both axial and torsional fatigue data to determine all of the model constants.

Experimental Details

Material and Specimens. Haynes alloy 188, 50.8-mm o.d., round bar stock that was hot rolled, centerless ground, and solution annealed was purchased from a commercial vendor. Table 1 shows the chemical composition of the alloy. Thin-walled tubular fatigue specimens (Fig. 1) were machined from

PRECEDING PAGE BLANK NOT FILMED

Table 1 Chemical composition of Haynes 188

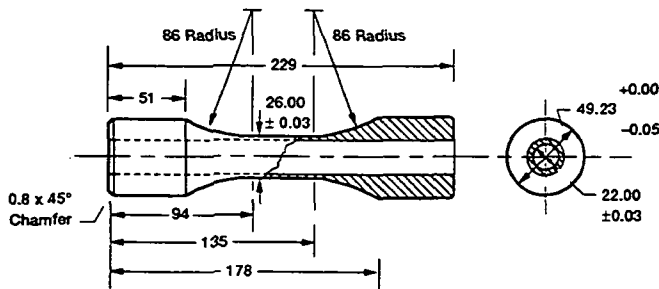| Element	Weight, percent
Sulphur	<0.002
Boron	.002
Phosphorous	.012
Carbon	.10
Silicon	.40
Lanthanum	.034
Manganese	.75
Iron	1.24
Tungsten	13.95
Chromium	21.84
Nickel	22.43
Cobalt	Balance

Fig. 2 Schematic of induction heating fixture

Fig. 1 Thin-walled tubular axial-torsional fatigue specimen (all dimensions are in mm)

the bar stock. The bores of the specimens were finished in a honing operation to help bias fatigue crack initiation to the outer surface of the tubular specimen (fatigue crack initiation from the internal surface was observed in a previous, room-temperature study by Bonacuse and Kalluri (1989)). All spec-
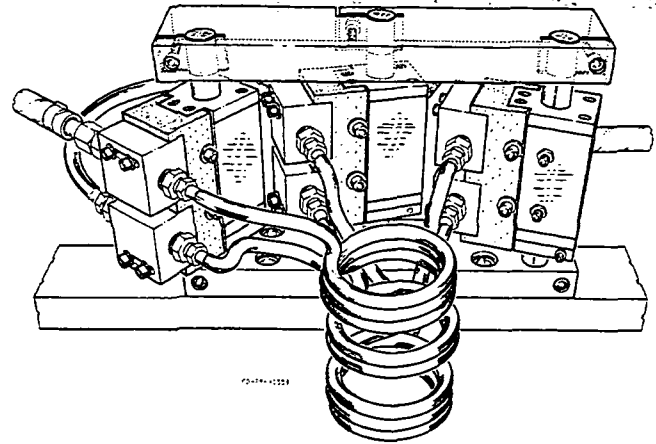
imens in this program had final failure cracks that initiated at the outer surfaces.

Test Apparatus. All tests were performed on a single servohydraulic axial-torsional test system under computer control. A commercially available axial-torsional extensometer equipped with quartz probes was used in all tests for strain measurement and control. Two indentations were pressed into the outer surface of the specimen with a precision fixture (developed at NASA Lewis Research Center) so that the conical tips of the extensometer probes could be mounted. A 50-kW induction heating system coupled to a movable three-coil heating fixture (Ellis and Bartolotta, 1990) was used to heat the fatigue specimens to the test temperature (Fig. 2). Every fatigue specimen loaded in the axial-torsional test system was located inside the three-coil heating fixture such that the center-coil of the heating fixture was at the middle of the gauge section and the upper and lower coils were just outside the gauge section. The heating fixture permitted adjustment of the heat input distribution, and thus allowed the thermal gradient within

Nomenclature

B, C = coefficients of axial elastic and plastic life relations

B', C' = coefficients of elastic and plastic life relations in Modified Multiaxiality Factor approach

B_t, C_t = coefficients of torsional elastic and plastic life relations

b, c = exponents of axial elastic and plastic life relations

b_t, c_t = exponents of torsional elastic and plastic life relations

E, G = Young's and shear moduli

K, K' = monotonic and cyclic axial strength coefficients

K_t, K_t' = monotonic and cyclic torsional strength coefficients

k = constant in Fatemi-Socie-Kurath parameter

MF, TF = multiaxiality and triaxiality factors

N_T = transition life

N_f = cyclic life

n, n' = monotonic and cyclic axial strain-hardening exponents

n_t, n_t' = monotonic and cyclic torsional strain-hardening exponents

α = mean coefficient of thermal expansion

γ, ϵ = engineering shear and axial strain amplitudes

γ_e, γ_p = elastic and plastic engineering shear-strain amplitudes

γ_{max} = maximum engineering shear strain

$\gamma_{xy}, \gamma_{yz}, \gamma_{zx}$ = orthogonal engineering shear strains

Δ = range of the variable

ϵ_T = transition strain amplitude

ϵ_e, ϵ_p = elastic and plastic strain amplitudes

ϵ_{eq} = von Mises equivalent strain amplitude

$\epsilon_{xx}, \epsilon_{yy}, \epsilon_{zz}$ = orthogonal normal strains

ϵ_f' = axial fatigue ductility coefficient

ϵ_1 = maximum principal strain

λ = ratio of engineering shear strain amplitude to axial strain amplitude, γ/ϵ

ν = Poisson's ratio

ν_e, ν_p = elastic and plastic Poisson's ratios

σ, τ = axial and shear stress amplitudes

σ_{eq} = von Mises equivalent stress amplitude

σ_f' = axial fatigue strength coefficient

σ_o, τ_o = mean axial and shear stresses

σ_y = axial yield strength

$\sigma_{xx}, \sigma_{yy}, \sigma_{zz}$ = orthogonal normal stresses

σ_n^{max} = maximum normal stress on the maximum shear strain plane

σ_1^{max} = maximum normal stress on the maximum principal strain plane

$\sigma_1, \sigma_2, \sigma_3$ = principal stresses

$\tau_{xy}, \tau_{yz}, \tau_{zx}$ = orthogonal shear stresses

Seven thermocouples (K-type chromel-alumel) are spot welded in a line parallel to the specimen axis 12.7 mm apart. This is duplicated on the opposite side of the specimen. Two thermocouples are also spot welded in the center of the gage section (90° around) as shown.
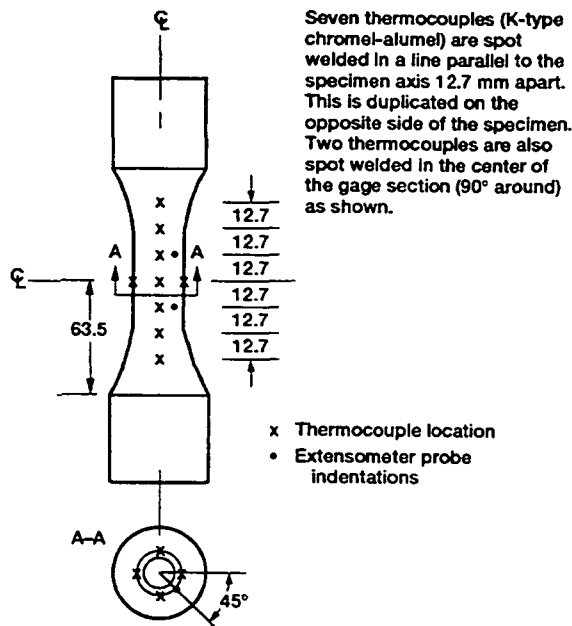
x Thermocouple location
• Extensometer probe indentations

Fig. 3 Thermocouple layout for measuring the temperature gradient in the tubular specimen (all dimensions are in mm)

O Young's
□ Shear
△ Handbook
$E(T) = -4.44 \times 10^{-5} T^2 - 0.0491T + 233$
$G(T) = -8.44 \times 10^{-6} T^2 - 0.0307T + 91.7$

Fig. 4 Young's and shear moduli versus temperature for Haynes 188

O Data
—— Polynomial fit,
$\alpha(T) = 1.4 \times 10^{-12} T^2 + 6.26 \times 10^{-9} T + 1.18 \times 10^{-5}$
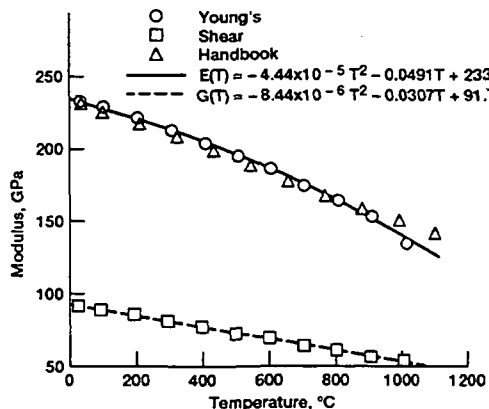
Fig. 5 Measured value of the mean coefficient of thermal expansion versus temperature for Haynes 188

the gauge section of each specimen to be kept to a minimum at any test temperature. Further details on the testing hardware and the computer test control and data acquisition system were documented by Bonacuse and Kalluri (1989) and Kalluri and Bonacuse (1990).

Young's Modulus, Shear Modulus, and Mean Coefficient of Thermal Expansion

The variations of E and G with temperature were determined by using a single specimen. Axial and torsional load excursions were performed at various temperatures starting at room temperature and progressing to 1000°C in increments of 100°C. The specimen was instrumented with thermocouples spot welded at 16 locations (Fig. 3) to monitor the temperature profile. Except for the highest control temperatures (900 and 1000°C), the temperature at each thermocouple within the gauge section was maintained to within 1 percent of the temperature (absolute) at the control thermocouple. The most deviant of the measured temperatures within the gauge section at the 900 and 1000°C test temperatures were greater by 1.25 and 2 percent of the control thermocouple temperatures, respectively. A fully reversed cycle in load control with a frequency of 0.1 Hz was used, and the peak loads were kept to 25 percent of the handbook value for the yield strength at each
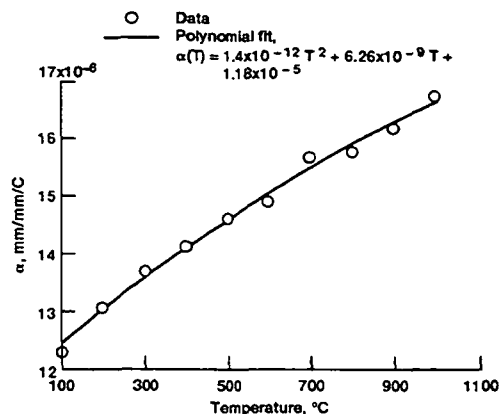
temperature tested. Linear least squares fits of the recorded stress and strain data were then performed to determine E and G. Figure 4 presents these test results and the second-degree polynomial least squares fits to the data of E and G versus temperature data. This figure also contains handbook values for the dynamic elastic modulus of Haynes 188 (Nickel Base Alloys, 1977). The experimental values obtained in this study closely agree with the handbook values except at the highest temperatures where the measured values were low, probably because of the slightly higher temperatures in the gauge section.

In the process of measuring the elastic properties, the axial thermal strain was measured by the extensometer and recorded. These data were used to calculate the value of α, with room temperature as a reference, for each increment in temperature. Figure 5 shows a plot of these data and the second-order polynomial fit to the data.

Axial and Torsional Tests

Haynes 188 exhibits a ductility minimum at 760°C (Nickel Base Alloys, 1977). Since low-cycle fatigue life is governed by the plastic strain range and the material's ductility, this temperature was selected to characterize the axial and torsional behavior of this material.

Monotonic Axial and Torsional Stress-Strain Behavior. Tensile and monotonic torsional tests were performed at 760°C to obtain the following: monotonic axial and torsional stress-strain curves; yield strengths in tension and in shear; ultimate tensile strength; and percent reduction in area (%RA) for Haynes 188 using the axial-torsional test configuration previously described. These tests were performed with the same thin-walled tubular specimen design as that used in the fatigue tests. In the tensile test a simple axial excursion was performed under strain control at a constant strain rate of 0.0008 s^{-1} (chosen to approximate the strain rate in the axial fatigue tests) to 4-percent axial strain. The specimen was then unloaded to zero; the extensometer was removed; and the specimen was reloaded in stroke control to complete separation. A stroke rate was chosen that would impart a strain rate roughly equivalent to that used in the strain-controlled segment.

The 0.2-percent offset yield and ultimate tensile strengths of the axially loaded specimen were 268 and 490 MPa, respectively. The area of the fractured surface of this specimen was measured to determine the tensile ductility. The %RA was 55.1, giving a tensile ductility of 0.801. The temperature profile of the specimen degraded by about 25°C as the length of the specimen increased by 27 mm and was pulled out of the induction heating coils. The observed increase in the length of the specimen was much smaller than the total heated length of specimen, which was about 120 mm. However, the degradation of the temperature profile of the specimen could have
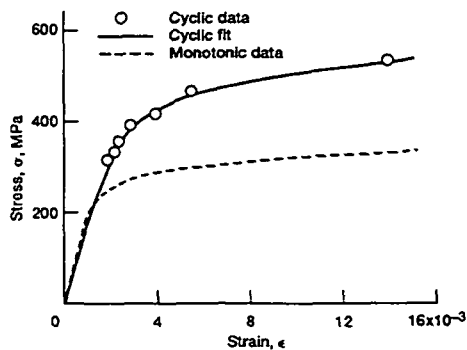
Fig. 6 Monotonic and cyclic stress-strain curves for Haynes 188 at 760°C
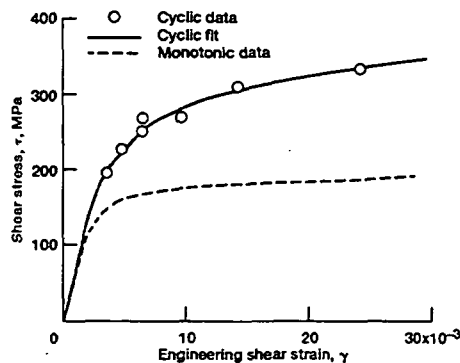

Fig. 7 Monotonic and cyclic engineering shear stress-strain curves for Haynes 188 at 760°C

introduced some error in the values of the ultimate tensile strength, the %RA, and the calculated tensile ductility.

A monotonic torsion test was performed to obtain the monotonic shear/stress behavior and the torsional yield stress of Haynes 188 at 760°C. This test was performed in shear strain control with a shear strain rate of 0.0006 s^{-1} (again, chosen to approximate the torsional fatigue test strain rates) to 3-percent torsional strain. The 0.2-percent offset torsional yield strength was 163 MPa. This test was not taken to failure for several reasons: (1) a commonly accepted monotonic torsional failure definition was not available; (2) the tube probably would have buckled before a shear crack could have formed; and (3) a monotonic shear failure could require hundreds of percent shear strain. Furthermore, if the test were actually taken to failure, the load frame used in this program would require that the specimen be ungripped and regripped many times (maximum rotation range is 100 deg) to put the required shear strain into the specimen.

Ramberg-Osgood type stress-strain relations were used to characterize the stress and strain data collected in these experiments:

$$\epsilon = \frac{\sigma}{E} + \left[\frac{\sigma}{K}\right]^{1/n} \quad \text{for monotonic axial test}$$

or

$$\gamma = \frac{\tau}{G} + \left[\frac{\tau}{K_t}\right]^{1/n_t} \quad \text{for monotonic torsional test} \quad (1)$$

The strain-hardening exponents and the strength coefficients were determined by fitting lines to the logarithms of the stress amplitudes versus the logarithms of the plastic strain amplitudes using least squares. The calculated values of K and n for the monotonic axial stress-strain curve were 512 MPa and 0.093, respectively. The calculated values of K_t and n_t for the monotonic torsional stress-strain curve were 264 MPa and 0.083, respectively.

Cyclic Axial and Torsional Stress-Strain Behavior. Cyclic axial ($\lambda = 0$) and torsional ($\lambda = \infty$) fatigue tests were conducted in air on Haynes 188 at 760°C. Triangular waveforms with a frequency of 0.1 Hz were used in both cases. The midlife (stabilized) stress amplitudes are plotted against the imposed strain amplitudes in Figs. 6 and 7 for the axial and torsional tests, respectively. Ramberg-Osgood type relations were used to characterize the axial and torsional cyclic stress-strain data:

$$\epsilon = \frac{\sigma}{E} + \left[\frac{\sigma}{K'}\right]^{1/n'} \quad \text{for axial fatigue tests}$$

or

$$\gamma = \frac{\tau}{G} + \left[\frac{\tau}{K_t'}\right]^{1/n_t'} \quad \text{for torsional fatigue tests} \quad (2)$$
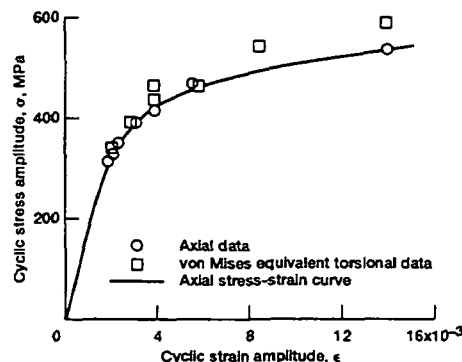

Fig. 8 Comparison of von Mises equivalent stress-strain data from torsional tests with axial stress-strain data

The values of K' and n', obtained by least squares analysis as described above, for the axial cyclic stress-strain curve were 891 MPa and 0.113. The values of K_t' and n_t', again obtained by least squares analysis, for the torsional cyclic stress-strain curve were 589 MPa and 0.142, respectively.

The monotonic axial and torsional stress-strain material response, obtained in the previously described experiments, are also plotted in these figures. Note that Haynes 188 exhibits considerable cyclic hardening in fully reversed loading at 760°C in both the axial and torsional fatigue tests. Leese and Morrow (1985) used a similar method to characterize the room temperature, cyclic, torsional stress-strain behavior for 1045 steel.

Comparison of Equivalent Stress-Strain Curves (Axial Versus Torsional). A traditional approach using von Mises equivalent strains and stresses was adopted to directly compare the torsional experiments with the axial experiments:

$$\epsilon_{eq} = \frac{1}{\sqrt{2}(1+\nu)} \left[(\epsilon_{xx} - \epsilon_{yy})^2 + (\epsilon_{yy} - \epsilon_{zz})^2 + (\epsilon_{zz} - \epsilon_{xx})^2 \right.$$
$$\left. + \frac{3}{2}(\gamma_{xy}^2 + \gamma_{yz}^2 + \gamma_{zx}^2) \right]^{1/2}$$

$$\sigma_{eq} = \frac{1}{\sqrt{2}} \left[(\sigma_{xx} - \sigma_{yy})^2 + (\sigma_{yy} - \sigma_{zz})^2 + (\sigma_{zz} - \sigma_{xx})^2 \right.$$
$$\left. + 6(\tau_{xy}^2 + \tau_{yz}^2 + \tau_{zx}^2) \right]^{1/2} \quad (3)$$

For pure torsion with the Poisson's ratio ν, assumed to be 0.5 (plastic strain-dominated, constant-volume assumption), the values of the equivalent strain and stress reduce to the following:

$$\epsilon_{eq} = \frac{\gamma}{\sqrt{3}}; \quad \sigma_{eq} = \sqrt{3}\,\tau \quad (4)$$

Figure 8 displays the von Mises equivalent torsional strain amplitude versus the von Mises equivalent stabilized torsional

Table 2 Axial fatigue data for Haynes 188 at 760°C

Specimen	$\Delta\epsilon_e$	$\Delta\epsilon_p$	$\Delta\epsilon$	$\Delta\sigma$, MPa	σ_o, MPa	N_f	Final crack length, mm
HY42	0.00635	0.02150	0.02784	1066	-5.30	94	>40
HY34	.00540	.00566	.01106	934	-6.17	625	6
HY32	.00482	.00287	.00768	832	-.70	1 420	14
HY39	.00466	.00135	.00600	786	-2.11	3 654	8
HY25	.00415	.00047	.00462	702	-.53	19 157	7
HY44[a]	.00394	.00024	.00416	658	4.93	35 106	4.5
HY43[a]	.00368		.00368	627	3.51	193 474	3-4

[a]Indentation cracking—data not included in computing axial fatigue life relation.

Table 3 Torsional fatigue data for Haynes 188 at 760°C

Specimen	$\Delta\gamma_e$	$\Delta\gamma_p$	$\Delta\gamma$	$\Delta\epsilon_{eq}$	$\Delta\tau$, MPa	τ_o, MPa	N_f	Final crack length, mm
HY8	0.01032	0.03868	0.04900	0.02829	667	1.74	259	>20
HY6	.00969	.01948	.02917	.01684	621	1.89	984	13
HY2[a]	.00844	.01122	.01966	.01135	536	1.59	2 194	13
HY5	.00799	.00515	.01314	.00759	533	1.74	2 268	22
HY7	.00779	.00542	.01321	.00763	504	2.04	4 933	26
HY3	.00717	.00255	.00972	.00561	455	1.74	18 043	26
HY4[a]	.00616	.00111	.00727	.00420	397	1.90	157 774	8

[a]Indentation cracking—data not included in computing torsional fatigue life relation.

stress amplitude. A comparison of these points with the axial cyclic stress-strain curve (also shown in Fig. 8) indicates that the material exhibits more cyclic hardening under torsional loading than is predicted by the von Mises criterion.

Fatigue Tests

The failure definition used for these experiments was a 10-percent drop off in the peak axial or torsional loads. The testing software stores the peak load values in a cycle at logarithmic intervals. These stored peak load values are used as a reference to compare with peak load values from subsequent cycles. The 10-percent load dropoff corresponded to surface crack lengths of 3 to 14 mm in the axial ($\lambda = 0$) fatigue tests (except in the largest strain amplitude test which had a crack of 40 mm) and surface crack lengths of 8 to 26 mm in the torsional ($\lambda = \infty$) fatigue tests.

Fatigue Data. Tables 2 and 3 contain stress and strain range values of the near half-life hysteresis loops of the axial ($\lambda = 0$) and torsional ($\lambda = \infty$) fatigue tests. These tables also include the final crack lengths (measured after the tests were completed). The extensometer probe indentations caused a problem in some of the specimens. These indentations were necessary to positively locate the extensometer probes on the specimen. In the longer life (lower strain range) tests, the crack that caused failure of the specimen occurred at an indentation. Fatigue data corresponding to the specimens that failed as a result of a crack at an extensometer indentation were excluded from the computation of the axial and torsional strain-life relations. In all tests the main crack followed a path perpendicular to the maximum principal stress direction.

Axial Fatigue Life Relations. The elastic and plastic strain ranges versus fatigue life data for the axial fatigue tests are presented in Fig. 9. Data points corresponding to specimens that failed as a result of a crack at the extensometer indentation are indicated with solid symbols. The elastic strain range was calculated for each test by using the measured Young's modulus and the recorded stress range. This value was then subtracted from the measured total strain range for that test to obtain the plastic strain range. Log-log fits were performed, excluding the data corresponding to the specimens that cracked at the indentations (solid symbols), on the calculated elastic and plastic strain ranges versus fatigue life. The calculated elastic, plastic, and total life relations are also presented in
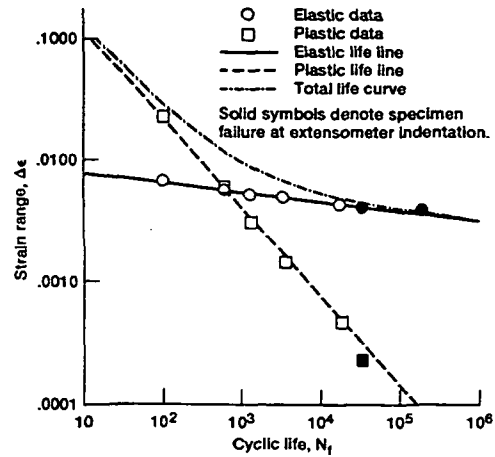

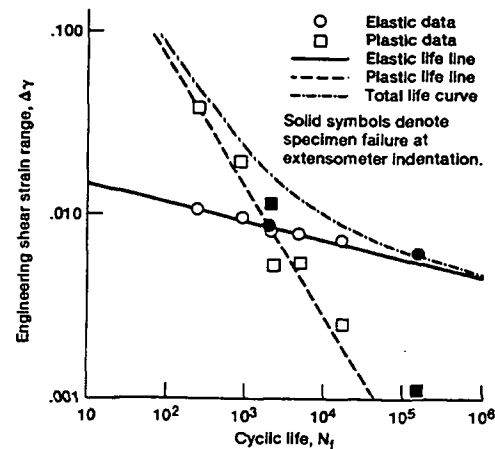**Fig. 9 Axial fatigue life relations for Haynes 188 at 760°C**

Fig. 10 Torsional fatigue life relations for Haynes 188 at 760°C

Fig. 9. The form of the axial strain-life equation is shown in Eq. (5).

$$\Delta\epsilon = B(N_f)^b + C(N_f)^c$$
$$= 0.00913(N_f)^{-0.0823} + 0.590(N_f)^{-0.730} \tag{5}$$

Torsional Fatigue Life Relations. For the torsional fatigue data, similar calculations were performed to separate the elastic and plastic engineering shear strain ranges. Log-log fits of the elastic and plastic engineering shear strain ranges versus fatigue life were performed. Figure 10 shows the elastic and plastic engineering shear strain range data and the corresponding life relationships. As with the axial fatigue data, data points corresponding to specimens with extensometer indentation cracking are indicated with solid symbols and were omitted from the computation of the torsional life relations. The torsional fatigue life relation is represented by the following:

$$\Delta\gamma = B_t(N_f)^{b_t} + C_t(N_f)^{c_t}$$
$$= 0.0184(N_f)^{-0.100} + 2.17(N_f)^{-0.715} \tag{6}$$

Leese and Morrow (1985) adopted a similar method to obtain the torsional fatigue life relations for 1045 steel at room temperature.

Analysis

Several multiaxial fatigue life prediction parameters (Manson and Halford, 1977; Socie, 1987; Fatemi and Socie, 1988, and Fatemi and Kurath, 1988) were selected to correlate the
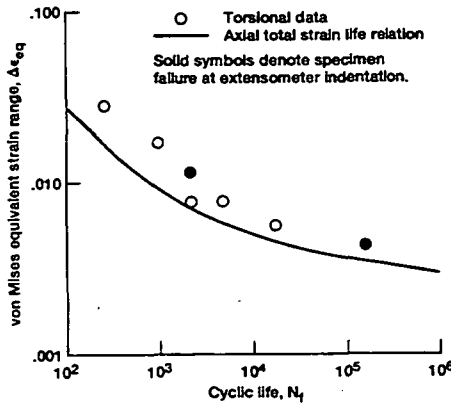
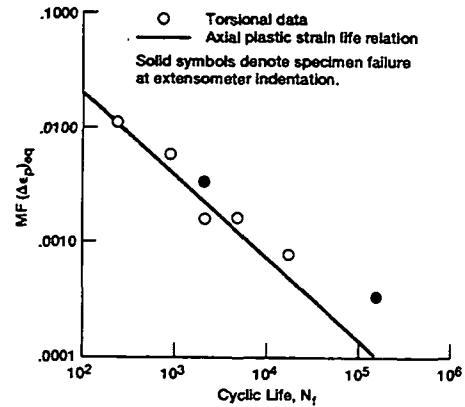**Fig. 11** Torsional fatigue life predictions by the von Mises equivalent strain range

Fig. 12 Torsional fatigue life predictions by the Manson-Halford parameter

high-temperature torsional fatigue life data for Haynes 188 at 760°C. All of these parameters, developed mainly to model room temperature multiaxial fatigue life behavior, require at least a uniaxial fatigue life data base to determine the respective model constants. Also, all fatigue life models examined cannot be solved in closed form for the fatigue life. An iterative solution is usually required. Results of the axial and torsional fatigue tests were used to derive the constants for multiaxial life prediction models and to gage the applicability of these models to Haynes 188 at elevated temperatures.

von Mises Equivalent Strain Range Parameter. This parameter uses the von Mises equivalent strain range (Eqs. (3) and (4)) taken from plasticity theory. For the torsional fatigue tests, the equivalent strain range is twice the equivalent strain amplitude computed using Eq. (4). This equivalent strain range is then used on the left hand side of the axial strain-life relation (Eq. (5)) to predict the torsional fatigue lives. As shown in Fig. 11, this model underpredicts the torsional fatigue life by a factor of 2 to 3. The von Mises equivalent strain range equation for Haynes 188 at 760°C is as follows:

$$\Delta\epsilon_{eq} = 0.00913(N_f)^{-0.0823} + 0.590(N_f)^{-0.730} \qquad (7)$$

Manson-Halford Parameter. Manson and Halford (1977) proposed a parameter that modifies the von Mises equivalent plastic strain range by a stress-based multiaxility factor which, in turn, is based on the triaxiality factor proposed by Davis and Connelly (1959). The equivalent plastic strain range for the torsional fatigue tests is twice the result of substituting only the plastic engineering shear strain amplitude into Eq. (4). The equivalent plastic strain range, modified by the multiaxiality factor, is then used in conjunction with the axial plastic life relationship to estimate the torsional fatigue life. The Manson-Halford parameter accounts for the change in the ductility of a material as the state of stress changes. This parameter for Haynes 188 at 760°C is given in Eq. (8).

$$MF(\Delta\epsilon_p)_{eq} = C(N_f)^c = 0.590(N_f)^{-0.730}$$

where,

$$MF = \frac{1}{2 - TF}; \quad TF \le 1$$

$$MF = TF; \quad TF \ge 1$$

and

$$TF = \frac{\sigma_1 + \sigma_2 + \sigma_3}{\frac{1}{\sqrt{2}}\sqrt{(\sigma_1 - \sigma_2)^2 + (\sigma_2 - \sigma_3)^2 + (\sigma_3 - \sigma_1)^2}} \qquad (8)$$

In torsion the triaxiality factor (TF) is zero ($\sigma_1 = -\sigma_2$, and $\sigma_3 = 0$) therefore, the multiaxiality factor (MF) is 1/2. This parameter works fairly well in the very low-cycle regime but is overly conservative (underpredicts the actual fatigue lives) as the amount of plastic strain decreases (Fig. 12). A total strain range verison of the Manson-Halford parameter, the Modified Multiaxiality Factor approach, has been developed by the authors to correct for this shortcoming.

Modified Multiaxiality Factor Approach. The functional form for this approach is obtained by employing the following assumptions. First, the hydrostatic stress (the triaxiality factor, and hence, the multiaxiality factor, is a measure of the hydrostatic stress) has a much greater effect on the axial plastic life line than the axial elastic life line, so that the multiaxiality factor is used to shift only the axial plastic life line as proposed by Manson and Halford (1977). Second, the axial elastic life relation is subsequently translated horizontally to preserve the cyclic axial stress-strain curve under different states of multiaxial stress. The form of the equation and the constants for torsional fatigue are as follows:

$$MF(\Delta\epsilon)_{eq} = MF^{(1-b/c)}B(N_f)^b + C(N_f)^c$$

$$= 0.00494(N_f)^{-0.0823} + 0.590(N_f)^{-0.730} \qquad (9)$$

Details of the development of Eq. (9) are presented in the Appendix. Figure 13 shows a plot of this equation with the torsional fatigue data. This equation predicts the low- and the high-engineering shear strain range data equally well.

Modified Smith-Watson-Topper Parameter. The conventions for the following two multiaxial fatigue life models are different from those used in the previously discussed models. The Modified Smith-Watson-Topper and Fatemi-Socie-Kurath models represent fatigue life in reversals-to-failure ($2N_f$) and express stresses and strains as amplitudes instead of ranges.

The Modified Smith-Watson-Topper parameter has been recommended by Socie (1987) for materials that exhibit an early transition to a tensile transgranular mode of failure. Originally presented by Smith et al. (1970) as a mean stress parameter, it was subsequently modified by Socie (1987) to model multiaxial fatigue life behavior.

$$\frac{\Delta\epsilon_1}{2}\sigma_1^{max} = \sigma_f'\epsilon_f'(2N_f)^{b+c} + \frac{\sigma_f'^2}{E}(2N_f)^{2b}$$

$$= 403(2N_f)^{-0.812} + 3.98(2N_f)^{-0.165} \qquad (10)$$

The exponents b and c are the same as the axial elastic and plastic line exponents for the fatigue life models previously discussed. The constants ϵ_f' and σ_f' are derived from the uniaxial fatigue data set. This fatigue life model along with
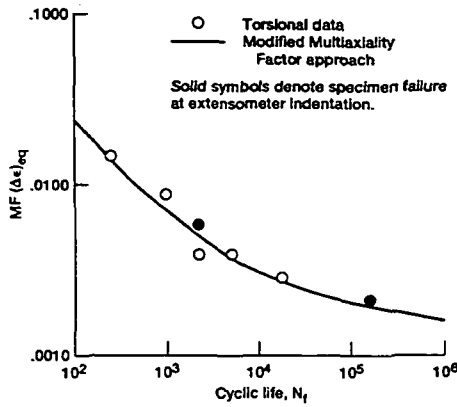
Fig. 13 Torsional fatigue life predictions by the Modified Multiaxiality Factor approach
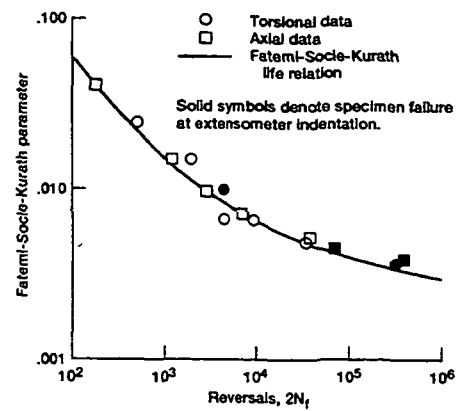

Fig. 15 Correlation of axial and torsional fatigue data by the Fatemi-Socie-Kurath parameter

preferentially oriented surface grains. This model successfully correlated the axial and torsional fatigue data.

Discussion

Several of the axial and torsional lower strain range fatigue tests developed cracks at indentations placed in the specimen surface for the extensometer probes. These indentations were necessary to ensure accurate mounting of the probes and to prevent movement relative to the surface over the course of a test. The precision indentation fixture allowed accurate control of the depth of penetration into the specimen's outer surface. The indentation depth was kept to the minimum necessary to prevent the probes from sliding at the maximum displacements expected in a given test. In pressing the indentations, residual stress fields are induced around the indentations. In the longer life tests these residual stress fields may relax to the point where they no longer prevent the stress concentration at the indentation from initiating a crack. Several specimen design alternatives that involve removing material from the gauge section between the extensometer indentations are under consideration. Such a modification to the specimen design should force the crack initiation site into this reduced gauge section. Elasto-plastic finite element analysis and experimental techniques could be used to account for the extra plastic strain that would occur in the reduced gauge section. Cracking at the extensometer probe indentations has been observed only in the experiments performed on Haynes 188 at 760°C. No such cracking was observed in previously conducted room temperature axial-torsional fatigue tests of similar strain ranges and performed on 304 and 316 stainless steels (Bonacuse and Kalluri, 1989 and 1993). These observations indicate that Haynes 188 at 760°C is more notch sensitive than the previously tested stainless steels.

At the highest axial and torsional strain ranges, the specimens exhibited small amounts of buckling. Fortunately, the specimen started buckling after the formation of a macroscale crack. To prevent buckling in future high strain range testing, a thicker-walled specimen will probably be necessary. The practical axial and torsional strain range limits for the specimen geometry used in this study are approximately 2.5 and 4.3 percent, respectively.

Among the multiaxial fatigue life prediction models examined in this study, the Modified Multiaxiality Factor approach provided good estimations of the torsional fatigue lives from uniaxial fatigue data. In particular, this approach eliminated the conservative predictions of the torsional fatigue lives by the Manson-Halford parameter at small strain ranges. In view of the fact that the main cracks followed paths that were perpendicular to the maximum principal stress direction in all fatigue tests, the reasons for the unconservative predictions (overprediction) of the torsional fatigue lives by the Modified Smith-Watson-Topper parameter are not clear at this time. As
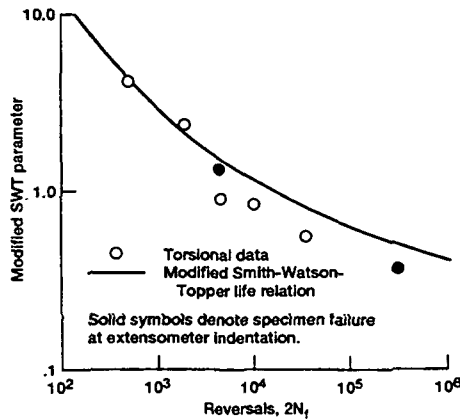

Fig. 14 Torsional fatigue life predictions by the Modified Smith-Watson-Topper parameter

the torsional fatigue data is depicted in Fig. 14. The Smith-Watson-Topper parameter does not model the torsional fatigue behavior of Haynes 188 very well. For the majority of the life range covered in this program, this model overpredicted the fatigue life by up to a factor of 6. This observation indicates that the Modified Smith-Watson-Topper model (at least for Haynes 188 at 760°C) is unsuitable for conservative design practice.

Fatemi-Socie-Kurath Parameter. The Fatemi-Socie-Kurath parameter (Fatemi and Socie, 1988 and Fatemi and Kurath, 1988) is included in this paper for future reference (Eq. (11)).

$$\gamma_{max}\left(1 + k\,\frac{\sigma_n^{max}}{\sigma_y}\right) = (1 + \nu_e)\,\frac{\sigma_f'}{E}\,(2N_f)^b + \frac{k}{2}\,(1 + \nu_e)\,\frac{\sigma_f'^2}{E\sigma_y}\,(2N_f)^{2b}$$

$$+ (1 + \nu_p)\epsilon_f'\,(2N_f)^c + \frac{k}{2}\,(1 + \nu_p)\epsilon_f'\,\frac{\sigma_f'}{\sigma_y}\,(2N_f)^{b+c}$$

$$= 0.00638(2N_f)^{-0.0823} + 0.00880(2N_f)^{-0.165}$$

$$+ 0.734(2N_f)^{-0.730} + 1.011(2N_f)^{-0.812} \quad (11)$$

For torsional fatigue tests, it is not a predictor of fatigue life as much as a correlator in that the torsional fatigue data are necessary to determine one of the constants (k). The method used to determine the parameter k from axial and torsional fatigue data was described by Fatemi and Kurath (1988). The value of k derived from this data set is 1.0 in the life regime of interest. Figure 15 shows a plot of the Fatemi-Socie-Kurath parameter values versus reversals-to-failure for the axial and torsional fatigue tests. In using the maximum shear strain as the dominant parameter, this model recognizes that the mode of crack initiation in most metals occurs by persistent slip in

previously stated, even though it may be nearly as accurate as the Modified Multiaxiality Factor approach, the Fatemi-Socie-Kurath parameter requires torsional fatigue data to obtain one of its constants.

Conclusions

The described fatigue test system configuration and multiaxial data acquistion and control software have been used to perform axial and torsional tests on Haynes 188 at high temperatures.

The multiaxial life models evaluated in this study estimate the torsional fatigue lives to varying degrees of accuracy. The von Mises equivalent strain range parameter was conservative (underpredicted actual fatigue lives) by up to a factor of 3 whereas the Modified Smith-Watson-Topper parameter was unconservative (overpredicted actual fatigue lives) by up to a factor of 6. The predictions by the Manson and Halford method were within a factor of 2 at larger strain ranges; however, at lower strain ranges they were conservative by up to a factor of 5. The Modified Multiaxiality Factor approach proposed in this paper rectified this problem and predicted all the torsional fatigue lives to within a factor of 2. The method of Fatemi, Socie, and Kurath correlated the axial and torsional fatigue data to within a factor of 2.5.

A modification to the specimen geometry may be necessary to avoid indentation cracking at lower strain ranges. Also, the small amounts of buckling that were observed at the higher strain ranges might be eliminated by adopting a specimen design with a thicker wall.

References

Bonacuse, P. J., and Kalluri, S., 1989, "Results of Inphase Axial-Torsional Fatigue Experiments on 304 Stainless Steel," AVSCOM TR 88-C-022, NASA TM-101464, National Aeronautics and Space Administration, Washington, DC.

Bonacuse, P. J., and Kalluri, S., 1993, "Axial-Torsional Fatigue: A Study of Tubular Specimen Thickness Effects," *Journal of Testing and Evaluation, JTEVA*, Vol. 21, No. 3, pp. 160–167.

Davis, E. A., and Connelly, F. M., 1959, "Stress Distribution and Plastic Deformation in Rotating Cylinders of Strain-Hardening Material," ASME *Journal of Applied Mechanics*, Vol. 81, pp. 25–30.

Ellis, J. R., and Bartolotta, P. A., 1990, "Adjustable Induction-Heating Coil," NASA Technical Brief, National Aeronautics and Space Administration, Washington, DC, Vol. 14, No. 11, p. 50.

Fatemi, A., and Kurath, P., 1988, "Multiaxial Fatigue Life Predictions Under the Influence of Mean-Stresses," ASME JOURNAL OF ENGINEERING MATERIALS AND TECHNOLOGY, Vol. 110, pp. 380–388.

Fatemi, A., and Socie, D. F., 1988, "A Critical Plane Approach to Multiaxial Fatigue Damage Including Out-of-Phase Loading," *Fatigue and Fracture of Engineering Materials and Structures*, Vol. 11, No. 3, pp. 149–165.

Kalluri, S., and Bonacuse, P. J., 1990, "A Data Acquisition and Control Program for Axial-Torsional Fatigue Testing," *Applications of Automation Technology to Fatigue and Fracture Testing, ASTM STP 1092*, A. A. Braun, N. E. Ashbaugh, and F. M. Smith, eds., American Society for Testing and Materials, Philadelphia, pp. 269–287.

Leese, G. E., and Morrow, J., 1985, "Low Cycle Fatigue Properties of a 1045 Steel in Torsion," *Multiaxial Fatigue, ASTM STP 853*, K. J. Miller and M. W. Brown, eds., American Society for Testing and Materials, Philadelphia, pp. 482–496.

Manson, S. S., and Halford, G. R., 1977, "Discussion, Multiaxial Low Cycle Fatigue of Type 304 Stainless Steel," ASME JOURNAL OF ENGINEERING MATERIALS AND TECHNOLOGY, Vol. 99, No. 3, pp. 283–286.

Manson, S. S., and Halford, G. R., 1981, "Correction: Practical Implementation of the Double Linear Damage Rule and Damage Curve Approach for Treating Cumulative Fatigue Damage," *International Journal of Fracture*, Vol. 17, No. 4, pp. R35–R42.

Nickel Base Alloys, 1977, International Nickel Company, Inc., New York.

Russell, D. A. et al., 1991, "Examination of the Effect of Propulsion System Performance Variables on the Life Prediction for the SSME LOX Post," *Structural Integrity and Durability of Reusable Space Propulsion Systems*, NASA CP 10064, National Aeronautics and Space Administration, Washington, DC, pp. 219–227.

Smith, K. N., Watson, P., and Topper, T. H., 1970, "A Stress-Strain Function for the Fatigue of Metals," *Journal of Materials*, Vol. 5, No. 4, pp. 767–778.

Socie, D. F., 1987, "Multiaxial Fatigue Damage Models," ASME JOURNAL OF ENGINEERING MATERIALS AND TECHNOLOGY, Vol. 109, No. 4, pp. 293–298.

APPENDIX

Development of the Total Equivalent Strain Range Version of the Multiaxiality Factor Approach

In low-cycle fatigue, under fully reversed uniaxial loading conditions, the Basquin and Manson-Coffin equations

$$\Delta\epsilon_e = B(N_f)^b \tag{12}$$

$$\Delta\epsilon_p = C(N_f)^c \tag{13}$$

adequately describe the fatigue life behavior of many engineering alloys.

The total strain-life relation is obtained by adding the Basquin and Manson-Coffin equations (Fig. 16).

$$\Delta\epsilon = \Delta\epsilon_e + \Delta\epsilon_p$$

$$= B(N_f)^b + C(N_f)^c \tag{14}$$

At the transition life, N_T, where $\Delta\epsilon_e = \Delta\epsilon_p$, the transition strain range, $\Delta\epsilon_T$, is given by

$$\Delta\epsilon_T = B(N_T)^b = C(N_T)^c \tag{15}$$

Solving Eq. (15) for the transition life, N_T, results in

$$N_T = \left[\frac{C}{B}\right]^{1/(b-c)} \tag{16}$$

Substituting Eq. (16) into Eq. (15) and solving for the transition strain range, one obtains

$$\Delta\epsilon_T = C\left[\frac{C}{B}\right]^{c/(b-c)} \tag{17}$$

Manson and Halford (1977) reasoned that under multiaxial loading conditions, the fatigue life of a material would be different from that under a uniaxial loading condition because multiaxiality can alter the ductility. Hence, they proposed that the von Mises equivalent plastic strain range be multiplied by a multiaxiality factor to account for the change in the ductility under multiaxial loading conditions. Their multiaxiality factor is a measure of hydrostatic stress and is based on the triaxiality factor of Davis and Connelly (1959). Thus, Eq. (13) under multiaxial loading becomes

$$MF(\Delta\epsilon_p)_{eq} = C(N_f)^c \tag{18}$$

or

$$(\Delta\epsilon_p)_{eq} = \frac{C}{MF}(N_f)^c \tag{19}$$

This equation deals only with the plastic portion of the von Mises equivalent strain range. In order to extend this approach to the total von Mises equivalent strain range, we propose that the following form of life relation be used for life prediction under multiaxial loading:
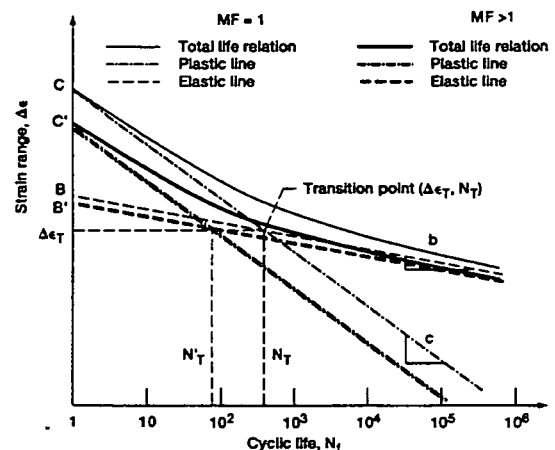

Fig. 16 Elastic, plastic, and total fatigue life relations under uniaxial ($MF = 1$) and Multiaxial ($MF > 1$) conditions

$$(\Delta\epsilon)_{eq} = B'(N_f)^b + C'(N_f)^c \qquad (20)$$

From Eq. (19),

$$C' = \frac{C}{MF} \qquad (21)$$

This implies that the plastic life line is moved down for $MF > 1$ (e.g., biaxial tension) and is moved up for $MF < 1$ (e.g., torsion). The new plastic life line is shown in Fig. 16 for $MF > 1$. The value of B' in Eq. (20) can be obtained by assuming that the cyclic stress-strain curve remains unchanged during multiaxial loading. It follows from this assumption that the transition strain range also remains unchanged. While this assumption may not be valid for all multiaxial loading conditions, it is at least consistent in that it uses both the uniaxial fatigue life relation and the corresponding cyclic stress-strain curve. The calculation of B' is accomplished by translating the elastic life line horizontally such that the transition strain range (Eq. (17)) remains the same. This method is analogous to the treatment of elastic and plastic life lines under different mean stress conditions by Manson and Halford (1981).

Thus,

$$\Delta\epsilon_T' = C' \left[\frac{C'}{B'}\right]^{c/(b-c)} = C \left[\frac{C}{B}\right]^{c/(b-c)} = \Delta\epsilon_T \qquad (22)$$

Substituting Eq. (21) into Eq. (22) and solving for B' yields[1]

$$B' = MF^{-b/c}B \qquad (23)$$

Substituting Eqs. (21) and (23) into Eq. (20) gives

$$(\Delta\epsilon)_{eq} = MF^{-b/c}B(N_f)^b + \frac{C}{MF}(N_f)^c \qquad (24)$$

Multiplying both sides of Eq. (24) by MF, the Modified Multiaxiality Factor equation is obtained:

$$MF(\Delta\epsilon)_{eq} = MF^{(1-b/c)}B(N_f)^b + C(N_f)^c \qquad (25)$$

Equations (24) and (25) constitute the basis of the Modified Multiaxiality Factor approach.

---

[1]An expression for B' involving MF was also reported by Russell et al. (1991). However, their expression is different from the one presented in Eq. (23). Also no experimental verification of the proposed equation was presented by Russell et al. (1991).